Biochar and activated carbons preparation from invasive algae Sargassum spp. for Chlordecone availability reduction in contaminated soils

Ronald Ranguin, Matthieu Delannoy, Christelle Yacou, Corine Jean-Marius, Cyril Feidt, Guido Rychen, Sarra Gaspard

Biochar and activated carbons preparation from invasive algae Sargassum *spp*. for Chlordecone availability reduction in contaminated soils

Ronald Ranguin [a, 1], Matthieu Delannoy [b], Christelle Yacou [a, 1], Corine Jean-Marius [a], Cyril Feidt [b], Guido Rychen [b], *, Sarra Gaspard [a], *

a : Laboratoire COVACHIMM2E, EA 3592, Université des Antilles, BP 250, 97157 Pointe-à-Pitre Cedex, Guadeloupe, France
b : Université de Lorraine-INRA (USC340), URAFPA, 54500 Vandoeuvre-lès-Nancy, France

Published in Journal of Environmental Chemical Engineering Available online: 25/02/2021 https://doi.org/10.1016/j.jece.2021.105280

Keywords

Sargassum; Activated carbon; Biochar; Chlordecone; Pollution sequestration; Food safety

Abstract

This work aims to valorize an invasive brown macroalga (Sargassum *spp*. consisting of two species Sargassum *fluitans* and Sargassum *natans*) by producing biochars (BCs) and activated carbons (ACs). Its abundant and frequent occurrence along the Caribbean coastlines, Florida, Gulf of Mexico during the last past nine years, have triggered human health concerns and have negatively impacted local economy, ecology and the environment. In this paper, BCs and ACs were developed to assess the reduction of chlordecone (CLD) environmental availability in artificial and tropical contaminated soils. Such innovative approach was proposed to limit CLD bio-availability to fauna and outdoor reared-animals. The BCs were prepared by pyrolysis at 700 °C while ACs samples by chemical or physical activation. Textural characterization, has evidenced that bi-modal structures with micro-and mesopores, various surface and high pore volumes were successfully obtained. Finally, the environmental availability tests resulted in various ability of BCs or ACs to significantly sequestrate CLD on artificial contaminated soils and on a natural nitisol. In particular, the BCs prepared with a 3 h pyrolysis time, exhibited the highest porosities properties and was the best candidate to efficiently sequestrate CLD in soil samples.

1. Introduction

In Guadeloupe Islands (French Antilles) and other Caribbean islands, washing ashore of tons of pelagic Sargassum spp. (i.e. *Sargassum* natans and *Sargassum* fluitans, a complex of two co-occurring species of floating brown macroalga), have been regularly occurring since 2011 [1]. Such events are more than likely due to both global warming and anthropic activities. For instance, the islands of Guadeloupe faced in 2019 one of its worst event that had never been described in the past. Algae dramatically accumulated on the beaches windward coastlines (Fig. 1). Hydrogen sulfide and ammonia gases are produced from the Sargassum decomposition, causing health effects and having indirect impacts on tourism, fisheries and recreational activities [2,3].

Recently, there has been a burgeoning trend in the Caribbean to transform such Sargassum *spp*. into added value matters. Herein, we propose to use this local and highly available resource to produce bio-chars (BCs) and activated carbons (ACs), thus contributing to solve the environmental problem of soils contamination by chlordecone (CLD) [4–6]. In fact, CLD was used during more than two decades (from 1972 to 1993) in the French West Indies, Africa and in other countries of central and South America, to treat banana plantations against the weevil *Cosmopolites sordidus* [7]. Whilst its toxicity

has been recognized since 1975, CLD was identified as a persistent organic pollutant only in May 2009 and as such was included in the Stockholm Convention on Persistent Organic Pollutants. The molecule has a high molecular weight (490.64 g mol-1), a very low solubility in water (2.7 mg L-1 at 25 °C), a high affinity for organic compounds (log Kow = 4.5) and is highly stable due to its caged chlorinated structure [8,9]. As a result, CLD can easily bind to soil particles and residues have been found in sediment layers as well as in various living organisms (i.e. human beings, animal and plants) from the land and coastal areas [10].

Unfortunately, the presence of CLD in water, soils and sediments of banana crops production zones, should last at least several decades up to seven centuries (for the most polluted Andosols) [11]. Therefore, in this work, the development of BCs and ACs derived from Sargassum *spp*. has been investigated to propose an eco-friendly opportunity of "biomass waste valorization" and an innovative strategy for limiting CLD bio-availability to fauna and outdoor reared-animals.

We have produced and characterized BCs and ACs, (with different textural and physico-chemical properties) to assess their potential for sequestering CLD in artificial and natural soils. While previous works have focused on using BCs to limit pollutants transfer [12–14], to improve soil water retention [15], for microbial activities [16] and to limit the volatility of nitrogen compounds needed for plant growth [17, 18]; few have examined the strategy of using BCs for preventing pollutant transfer to livestock. Recent papers [19–21] have reported on the great potential of ACs and BCs to sequestrate CLD in Antillean soil. In our previous work, the amendment of Nitisol by lignocellulosic ACs, such as Coconut shell or Oak wood which resulted in significant reductions of CLD-availability [21]. However, to our knowledge, no sequestration data are currently available concerning BCs or ACs derived from Sargassum spp.

2. Material and Methods

2.1. Preparation of activated carbons from raw material

French West Indies) in July 2017. The samples were initially dried at room temperature and then in an oven at 105°C for 48 h to remove the moisture content. They were then grounded and finally sieved into several fractions [22]. The fraction containing particle size ranging from 0.4 to 1 mm was selected as precursor for producing the ACs and BCs. In this work, BCs were obtained from the pyrolysis of the Sargassum spp. precursor (i). The ACs were obtained either by physical activation of BCs (ii), or by chemical activation (iii) [22].

(i) Sargassum spp. precursor was pyrolysed in a nacelle which was placed in a tubular furnace (Carbolite Gero® CTF 12/75/700) under a nitrogen flow of 80 mL min^{-1} at 700 °C for 1 h or 3 h, with a heating rate of 10°C.min^{-1}. The pyrolysis temperature chosen is that for which the yield η(%) remains constant [23].

Where
wi weight of initial dry precursor (g).
wf mass of carbon after pyrolysis (g).

$$\eta(\%) = 100 \times (wi - (wi - wf))/ wi \quad (1)$$

After the pyrolysis, the as-prepared BCs were washed under a fume hood with HCl (5 M) to remove impurities. Subsequent washing was carried out with deionized water (10 µS cm- 1) in a beaker with stirring, until pH of 6–7 was reached [24,25]. Samples were finally purified by Soxhlet extraction during 24 h with deionized water, giving rise to BCs labeled BioSarg 1 h and BioSarg 3 h, depending on the pyrolysis time.

(i) For physical activation, approximately 3 g of BioSarg 1 h was heated at 10 C min- 1 to the final temperature of 600 °C with carbon dioxide (CO2), a CO2/H2O mixture and steam (H2O), using nitrogen as carrier gas at a flow rate of 80 mL.min- 1, during 19 h, 20 h or 14 h respectively. Different time span and a temperature of 600 °C were chosen to reach a burn-off of approximately 50% and avoid the eventual collapse of some pore walls in the core of the ACs [26].

Samples were labeled SargCO2, SargCO2/H2O and SargH2O. The burn-off (%) refers to the percentage of mass loss, which indicates efficient activation [27,28]. This is calculated according to the following equation:

$$\ll\text{burn - off}\gg\% = 1 - W_{final}/W_{initial} * 100 \quad (2)$$

with

$W_{initial}$ weight of initial dry BCs (g).
W_{final} mass of carbon after activation (g).

(i) Chemical activation was carried out with approximately 9 g of Sargassum spp. precursor. For this purpose, the latter was impregnated in phosphoric acid (H_3PO_4, 85 wt%) for 24 h to ensure optimal wettability, resulting in an impregnation ratio of 0.5:1 (g H_3PO_4/g precursor) [22]. Thereafter, the samples were dried in an oven at 110 ˚C during 4 h, followed by a pyrolysis step using the same conditions as those described in BCs preparation. After cooling, until ambient temperature, the ACs thus obtained were washed with distilled water until stabilization of the pH, and then dried overnight using a drying oven at 110 ˚C.

In our study, chemically activated samples are referred to as SargP0.5.

2.2. Characterization of the ACs and BCs

Thermogravimetric analysis was carried out using a Labsys Evo-Setaram instrument from 35° to 900°C at a rate of 10 °C.min^{-1}, under an inert nitrogen atmosphere flow of 80 mL min^{-1}. The morphological features of samples were analyzed by scanning electron microscopy (SEM, Hitachi S-2500, accelerating voltage of 20 kV).

Textural properties of ACs and BCs were determined using a Micro-meritics ASAP 2020 apparatus. Prior to analysis, the samples were degassed for 24 h at 300 °C. To estimate the surface area $_{(SBET),}$ the Brunauer, Emmett and Teller (BET) model [29] was utilized and the Dubinin–Radushkevich (D-R) equation was used to determine micro-porous volume [30]. The mesoporous volume was estimated by applying the Barrett–Joiner–Halenda (BJH) method on the desorption branch [31,32].

Raman spectroscopy analysis was determined using a HR 800 Horiba multi-channel spectrometer.

FT-IR spectra were collected using a Perkin Elmer Spectrum One FT-IR Infrared Spectrometer, equipped with an ATR sampling accessory (diamond/ZnSe composite crystal). The spectra were recorded in a range of 4000–550 cm^{-1}.

X-ray photoelectron spectroscopy was investigated using a Kratos

2.3. Assessment of CLD sequestration potential of Sargassum biochars and ACs

In this study CLD sequestration efficiency of each Sargassum BCs or ACs was assessed through environmental availability assays, which allow to determine the CLD part which may be extracted by fauna or biota as described in [21]. These assays were first applied to artificial soils in order to select the most efficient Sargassum BCs or ACs. In a second step, the most efficient sargassum BCs was added to an Antillean CLD contaminated nitisol.

2.3.1. Environmental availability assays

Environmental availability assays were performed on each artificial and natural soil sample. The protocol was adapted from the XP ISO/TS 16 751 Part B to fit a 2 g soil-sample instead of 5 g as previously described [21]. Briefly, 600 ± 25 mg of Tenax® (60–80 mesh, Sigma-Aldrich, Saint-Louis) and 28 mL of ultrapure water were added to soil samples. After a 20 h agitation period Tenax® was recovered and then extracted 3 times with acetone (LV-GC, Biosolve, Lyon) using an ultrasonic bath. All extracts were combined and concentrated prior GC-MS analyze (Agilent 7890) to quantify CLD content.

2.3.2. Artificial soils preparation

Artificial soils were prepared accordingly to the OECD guideline 207 [33] as described in [21]. All artificial soils were spiked to reach a concentration of 5 µg of CLD (Kepone, Supelco, Sigma Aldrich, Saint-Louis) per g of DM. Then BCs or ACs were added (2% dry mass basis of whole soil) and hand-mixed thoroughly. All artificial soils were aged during 80 days prior the following experimental parts [21].

2.3.3. Nitisol amendment

Nitisol sample preparation and amendment were performed as described in [21]. Briefly, Nitisol contaminated soil was sampled in Guadeloupe [34] and dried at room temperature until mass stabilization. Then, 2% of the most efficient condensed materials (dry mass basis) was added to 2 g subsamples of this soil ($n = 3$). Six non-amended subsamples were used as control. Finally, ultrapure water was added to reach 18% of mass of the wet soil. All soils were aged during 80 days at room temperature (20 ± 2 ˚C) prior the following experimental parts.

2.3.4. Statistical analysis

In order to assess the impact of sargassum BCs and ACs on CLD environmental availability, an ANOVA was performed. The ANOVA procedure and the Tukey–Kramer post-hoc test of R version 3.2.3 (R Foundation for Statistical Computing, Vienna, Austria) were used. Differences were considered significant at $P < 0.05$.

3. Results and Discussion

3.1. Characterization of the ACs derived from Sargassum fluitans

3.1.1. Thermogravimetric behavior

To anticipate AC and BC samples preparation procedure, thermal behavior of the sargassum precursor was studied by a thermogravimetric (TG) technique. Fig. 2(a) shows TG (weight loss, %) and DTG (derivative of TG) curves, while Fig. 2(b) shows the corresponding DSC (differential scanning calorimetry) curve with both endo- and exothermic peaks. Analysis of these thermograms revealed three different stages of the alga degradation: (i) stage I - from initial temperature to 150 ˚C, (ii) stage II - between 200 and 400 ˚C and (iii) stage III - from 450 ˚C to 900 ˚C. During the first stage, an endothermic peak was observed (at around 135 ˚C), which could correspond to the desorption of both cellular water and external water bound by surface tension. This represents a total mass loss of 4.3 wt% (calculated from the TG plot). In the second stage, the main pyrolytic process occurred and majority of weight loss was observed. The DSC curve shows an endothermic peak at 212 ˚C followed by an exothermic peak at 270 C, corresponding to a mass loss of 8.6 wt% and 27.7 wt%, respectively. Previous work has shown that those phases could be attributed to the removal of alginic acid and fucoidan, two major constituents of algal biomass [35,36]. The following mass loss of 39.1 wt%, at around 328 ˚C, can be assigned to the decomposition of other carbohydrates [37]. Third stage starting from 450 ˚C with an endothermic effect, was probably caused by the loss of volatile metal and by carbonate decomposition [38,39]. Such multi-compounds decomposition of Sargassum spp., at temperature below 700 ˚C, suggests a complex structure. It should be noted that after 700 ˚C, no significant weight loss was observed, thereby suggesting thermal stability of the sample was reached. Therefore, a pyrolysis temperature of 700 ˚C can be chosen for the BCs preparation.

3.1.2. Scanning electron microscopy (SEM)

Surface morphology of the Sargassum samples was analyzed by scanning electron microscopy (SEM) as shown in Fig. 3. A relatively dense sample surface with rod-like tissues could be observed, which essentially contains the proteins and cell wall of the algae (Fig. 3a). Unlike lignocellulosic precursors, it seems that the brown alga does not have macropores intrinsic to its matrix, which is probably due to its limited fibrillar microstructure [40]. Upon pyrolysis, the sample underwent microstructural modification, as indicated by the appearance of a rough surface in which macropores were clearly identifiable (Fig. 3b, c). Such thermal treatment has successfully led to release volatile compounds contained in the seaweed, giving rise to a porous structure. However, at such magnification, it is clear that SEM analysis did not provide evidences of the presence of smaller micropores that could participate to CLD sequestration. This feature will be discussed in the next sections using appropriate characterization techniques.

3.1.3. BET analysis

Adsorption/desorption of N2 at 77 K was measured for the BCs and ACs Sargassum *spp*. and the corresponding isotherms are displayed in Fig. 4. Hysteresis loops were observed in all samples (except for BioSarg 1 h), indicating type IV isotherms according to the classification established by De Boer et al. [41]. The well-defined hysteresis loops (especially observed for BioSarg 3 h and SargP0.5), which taken in conjunction with the initial uptake of volume adsorbed at low partial pressure ($P/P_0 < 0.2$); indicated that the pore size distribution for these samples was bimodal with both micro- and mesopores present. On the other hand, BioSarg 1 h exhibited a type I isotherm, characteristic of exclusively microporous materials. Such trends were confirmed by analyzing the textural parameters (specific surface area, pore volumes and pore width) depicted in Table 1. BioSarg 1 h exhibited only micropores combined with the lowest total volume ($VT = 0.019\ cm^3$), while BioSarg 3 h and SargP0.5 contained both micropores and meso-pores combined with highest total volumes ($VT = 0.99$ and $0.76\ cm^3\ g^{-1}$). One can note that, comparison of BioSarg 3 h and Biosarg 1 h clearly shows the influence of the pyrolysis time as more porosity was developed in Biosarg 3 h. In addition, BioSarg 3 h exhibited one of the largest pore size ($DP = 4.54$ nm) whilst BioSarg 1 h the lowest one ($DP = 1.56$ nm). It is

expected that such features of BioSarg 3 h could contribute to enhance CLD bioavailability [21]. Finally, in term of surface areas, the descending order was as follows: SargCO_2 > SargP0.5 > BioSarg 3 h > SargH_2O > Sarg H_2O/CO_2 > BioSarg 1 h. The physically activated SargCO2 has the largest surface area (SBET = 969 m2.g^{-1}) with a large fraction of small mesopores compared to its microporous volume.

3.1.4. Part 2

ACs and BCs microstructures were characterized by Resonance Raman spectroscopy and the spectra are shown in Fig. 5. The Raman "G" peak referring to the bond-stretching vibrations of sp2 carbon sites is generally found around 1580 cm^{-1} in crystalline graphite [42]. The "D" peak at around 1355 cm^{-1} is a signature of disorder and/or defects in diamond carbon and amorphous carbon due to sp3 breathing vibrations [43,44].

The D-mode is attributed to lattice defects and finite crystal size occurring inside the graphene atomic layer which induce a breaking of the 2D translational symmetry [45]. ID/IG represents the ratio R of the integrated intensity of the D mode (ID) over that of the G mode (IG) deduced from the Raman analysis. R is commonly used to characterize disorder in graphene and has usually the same trend as the ratio of the area under the D-peak over that under the G-peak [46]. BCs have the highest ID /IG ratio = 1.04 and 1.02 (Table 2). This means that the D band is related to formation of defects (disorder) and a high proportion of sp3 carbon and results from breaks in the sp2 hybridized (out of plane) carbon bonds [47], according to the fact that BCs are only submitted to a one step pyrolysis [21].

3.1.5. FTIR spectroscopy

To identify chemical surface groups of the prepared samples, FT-IR spectroscopy was carried out. Fig. 6 shows the resulting spectra of the ACs (SargP0.5, SargCO_2, SargH_2O and Sarg CO_2/H_2O) along with that of BCs (BioSarg 1 h and BioSarg 3 h). It is clearly seen that there are similarities and differences in chemical makeup by comparing the BCs and ACs samples.

In ACs spectra, features bands were identified: (i) at 2981 and 2930 cm^{-1} which are associated with asymmetric and symmetric CH2 stretching vibrations, respectively; (ii) between 1400 and 1600 cm^{-1} which are ascribed to the skeletal C=C vibrations in aromatic rings bands; (iii) at around 1400 cm^{-1} which can be partially described by OH deformation vibration; (iv) in the region of 1350–1200 cm^{-1} which can be attributed to C–O–C vibrations; (v) at 871 cm^{-1} can be attributed to C=CH2 bending out of-plane [48,49].

In BCs spectra, characteristic bands were identified at 1200 and 1530 cm^{-1} which can be related to the hydroxyl and C-O-C groups stretching vibration in pyranose ring skeletal or stretching in aromatic ring and C=C groups (sp2-hydridized carbon) respectively [50].

We have to bear in mind that ACs prepared py physical activation were produced from BCs (activation of BioSarg 1 h with steam or CO2). The significant absorption band in the region 1350–1200 cm^{-1}, suggests that the activation with steam or CO2 favored the development of C-O groups on the surface of the ACs. This agrees well with observation reported in literature [51,52]. Overall, FT-IR results showed that the differences in surface chemistry of the ACs are relatively small and could lead to similar effect in the reduction of CLD bioavailability.

3.1.6. X-ray photoelectron spectroscopy (XPS)

The produced ACs and BCs were further analyzed via XPS spectroscopy to identify chemical elements and functions present on their surfaces. As shown in Table 2, the main elements detected are O, Na, Cl, Ca, S, Mg, Si and C, which correspond to typical marine residues [35]. Although the as-prepared samples were thoroughly washed in deionized water, persistence amounts of salt (NaCl) remain in some of the sample matrices (i.e. BioSarg 3 h, SargCO_2, SargH_2O/CO_2 and SargH_2O). Noteworthy, the salt content was higher in sample SargCO_2 than for those activated with steam (SargH_2O and SargH_2O/CO_2). This suggests that the activation with water vapor preferentially removes the NaCl during the process. This is supported by the fact that steam activation requires less energy than CO_2 activation as shown in Eqs. (2) and (3) SargH_2O/CO_2 sample confirms this trend due to the competition between the CO_2 and H_2O molecules as shown in Eq. (4).

$$C(s) + H2O(g) \rightarrow CO(g) + H2\ (g) \Delta H298K = +\ 117 kJ.mol^{-1} \quad (2)$$

$$C(s) + CO2(g) \rightarrow 2CO(g) \Delta H298K = +\ 159 kJ.mol\text{-}1 \quad (3)$$

$$CO2\ (g) + H2O(l) \rightarrow H2\ CO3(g) \Delta H298K = +\ 2.20 kJ.mol^{-1} \quad (4)$$

As seen in Table 2, the ratio O1s/C1s increases by 1.5 fold when comparing SargH2O against SargCO2, indicating that during the activation

process, additional oxygenated functional groups were formed

However, the activation with H2O/CO2 mixture, shows an opposite effect, as the ratio O1s/C1s decreased by a factor close to 0.6. This observation is in good agreement with the work published by Mangun et al. [55], where the oxidation steps during physical activation were described as follows:

$$-CH \rightarrow -C-OH \rightarrow -C-O- \rightarrow -COOH \quad (5)$$

The deconvolution (not shown here) of the C1s spectrum consists of five components with binding energies corresponding to (i) the graphite type and amorphous carbon (C-C, C-H) at 284.6 eV, (ii) carboxyl and ester groups (O-C) at 285.7 eV, (iii) carbonyl group (O=C) at 287.2 eV, (iv) acidic group (O = C-OH) at 289.7 eV, (v) and a peak at around 292.1 eV belonging to the π-π *transition band (HOMO-LUMO) in the aromatic carbon [56,57]. The O1s oxygen peak spectrum was also deconvoluted into two peaks at 531.4 eV and 532.9 eV. The peak at 531.4 eV can be ascribed to the oxygen attached to the carbonyl group (O = C) and the peak at 532.9 eV can be attributed to the oxygen in the epoxy and/ or hydroxyl (C-O-C, C-O - H) [58].

According to the results presented in Table 2, BioSarg 1 h and Bio-Sarg 3 h showed a higher content of disordered carbons C-C, C-H (54.39% and 74.34%, respectively) than the ACs materials. This correlates well with the RAMAN analysis, which showed that ACs matrices were the most structurally organized (with lowest % of disordered carbon ranging from 47.92% to 49.24%). In addition, ACs sample made by physical activation reveals a slightly higher percentage of carbonyl groups (C=O, O-C=O, HO-C=O). (Table 3).

3.2. Assessment of CLD sequestration potential of sargassum biochars and ACs

The first set of assays involved 7 OECD soils amended by one of the Sargassum ACs or BCs. The results are presented in Fig. 7. One of the significant figures is that 84.2 ± 2.1% of the whole CLD content was retrieved from Artificial soils (n = 6) without amendment indicating that the main part of soil CLD was easily available. No significant reduction of CLD availability was observed when the artificial soils were amended by the different Sargassum ACs or by BioSarg 1 h. The obtained values are ranging from 69% to 96% of environmental availability. Interestingly, a much better response ($p < 0.001$) was obtained when the artificial soil was amended by the BioSarg 3 h (17% of CLD environmental availability compared to 84.2% without amendment). This reduction corresponds to 4/5 reduction of CLD environmental availability compared to the non-amended artificial soil.

In the second set of assays, a naturally contaminated Nitisol sample amended by BioSarg 3 h was studied. Significant reduced level of environmental availability was observed similarly to as in artificial soils, revealing the great sequestration potential of this BCs (Fig. 7). Thus, BioSarg 3 h presented more than 80% reduction of CLD environmental availability in Nitisol (19% environmental availability), confirming the effectiveness of this amendment to sequester CLD even in a contaminated soil.

3.2.1. Impact of Sargassum ACs or BCs characteristics on CLD sequestration

Interestingly, the present study reveals that one BCs (BioSarg 3 h), was able to efficiently sequestrate CLD, either in the OECD artificial soils or in the CLD contaminated Nitisol. In contrast to previous results obtained from lignocellulosic precursors, where the BCs did not present a strong sequestration potential [21], the BioSarg 3 h used in this study appears to be a valuable candidate for this purpose. Indeed, BCs is prepared in an eco-friendly way with a unique pyrolysis step that may induce, even if the sample must be effectively washed, a reduced cost of preparation at industrial scale when compared to physical or chemical activation.

The explanation of the sequestration capabilities is related on the fact that BioSarg 3 h exhibits numerous interesting characteristics when compared to others samples. Indeed, textural characteristics like specific BET surface area, total pore volume, and micro- and mesopore volume and mean pore diameter were the highest when compared to all other BCs and ACs. These physico-chemical characteristics are well known to play a major role for organic pesticide sequestration [21]. CLD availability reduction is far much higher that the values obtained for samples SargP0.5, SargCO2 that exhibited as well a high surface area value. In addition, textural properties like micro- and mesopore volumes appear also to play a role in this reduction. Indeed SargCO2 has the highest surface area of 968 $m^2.g-1$, but was not able to retain CLD in this study, that may be due to the very low amount of micropores that may entraps CLD. Indeed, the BioSarg 3 h displayed a high proportion of micropo-rosity and mesoporosity compared to the other matrices. A similar

observation was also previously noticed in another set of BCs and ACs [21,59]. On the other hand SargP0.5 that contains as well micropores in slightly lower quantity than BioSarg 3 h is not able to retain significantly CLD. Even with a very low surface area, and low micropore volume, SargH2O gives a CLD availability reduction of 32%, showing that textural characteristic is not the only factor affecting CLD sequestration by carbon material. Chemical groups at carbon samples, may as well play a role in CLD availability reduction in soil. Indeed, surface chemistry is known to play a major role in chlorinated pesticides adsorption in water, for example [60,61] that is not observed in the present work, where CLD is removed from soil instead of water. Although several surface characterizations were carried out in this work, no conclusion could be drawn at this stage concerning the relationship between surface chemistry and CLD-bioavailability.

Overall, these results suggest that a significant CLD environmental availability reduction can be expected only when the condensed material is highly porous but it depends as well on other factors. Therefore, influence of carbon chemistry, that includes surface groups polarity, acido-basic character, which are dependent on soil characteristics such as soil pH, moisture, etc., needs further investigations.

4. Conclusion

This study revealed that pyrolysis of Sargassum spp. can result in condensed materials with high level of porosities. In particular, BioSarg

3 h (Sargasum precursor pyrolysed during 3 h) displayed both the highest total volume in pore and one of the best BET surface. Thus, this biochar appeared to be the best candidate to sequestrate efficiently CLD in soil samples, suggesting that textural properties of the materials played a major role. This really promising result indicates that a wider use of this biochar, with a lower preparation cost and easy preparation process, could contribute to strongly limit the CLD transfer to the food chain. Additional works (i.e. influence of pH soils, effect of CLD loading in soils, contact time, etc.) are now in progress to provide better understanding of the obtained results. Overall, these results can be considered as a major first step toward further bioavailability assays aiming to study CLD transfer from soils to both plants and food producing animals.

Acknowledgements

We thank Harry Archimède (INRA Antilles-Guyane) for initiating the collaboration between Université des Antilles, COVACHIMM2E Laboratory and Université de Lorraine-INRA, URAFPA. We also thank Sandra Roche for participating to technical support. Post-doctoral and Ph.D. stipends was provided by Region Guadeloupe-FEDER 2014–2020. We acknowledge the financial support of PNAC3-PITE convention no. DRRT-2015-02) and the ANR (ANR-16CE210008-01).

Declaration of Competing Interest

The authors declare that they have no known competing financial interests or personal relationships that could have appeared to influence the work reported in this paper.

Table 1. Textural parameters of Sargassum spp. BCs and ACs calculated from N_2 sorption analysis.

Sample	Burn-off (%)	BET Surface area (g^{-1})	$V_{Micropores}$ (D-R) (cm^3. g^{-1})	$V_{Mesopores}$ (BJH) (g^{-1})	Total volume in pore (g^{-1})	Average pore width Dp (nm)
BioSarg 1 h	72	54	0.021	–	0.019 (NLDFT[a])	1.56
BioSarg 3 h	70	872	0.44	0.55	0.99	4.54
SargP0.5	51	877	0.30	0.46	0.76	3.46
Sarg H_2O/ CO_2	47	80	0.10	0.36	0.46	2.29
Sarg H_2O	46	109	0.12	0.09	0.13	4.79
Sarg CO_2	46	969	0.041	0.34	0.38	1.57

[a] NLDFT: Non-local density functional theory.

Table 2. Calculated ID/IG ratio, graphitic and disordered carbon proportions in ACs and BCs samples.

Sample	BioSarg 1 h	BioSarg 3 h	SargP0.5	SargCO_2	SargH_2O	SargH_2O/CO_2
I_D/I_G	1.02	1.04	0.94	0.96	0.97	0.92
% graphitic carbon	49.50	49.02	51.55	51.02	50.76	52.08
% disordered carbon	50.50	50.98	48.45	48.98	49.24	47.92

Table 3. Atomic concentration (%) of the chemical elements and functional groups present Sargassum spp. BCs and ACs surfaces (obtained from XPS spectra).

	Atomic Concentration (%)															
Sample	Na 1 s	O 1 s	Ca 2p	C 1 s	Cl 2p	Mg 2p	S 2p	Si 2p	O 1 s/C 1 s	C-C; C-H	C-O	C=O	O-C=O	HO-C=O	π–π*	π∂
BioSarg 1 h	16.93	32.98	6.69	30.41	9.13	–	3.87	–	1.08	54.39	29.26	16.35	–	–	–	–
BioSarg 3 h	–	46.29	–	28.71	–	15.08	–	9.93	1.61	74.34	19.13	6.52	–	–	–	–
SargP0.5	–	41.41	7.89	32.34	–	8.25	8.08	2.03	1.28	–	–	–	–	–	–	–
SargCO2	25.37	19.53	7.11	23.01	21.01	3.49	–	–	0.85	48.19	25.71	–	26.11	–	–	–
SargH2O	11.83	22.78	9.31	41.27	9.44	3.89	1.46	–	0.55	46.23	10.66	26.19	–	–	12.33	4.56
SargH2O/CO2	10.7	23.72	–	49.26	8.52	6.71	1.10	–	0.48	48.6	24.27	14.1	–	5.63	7.4	–

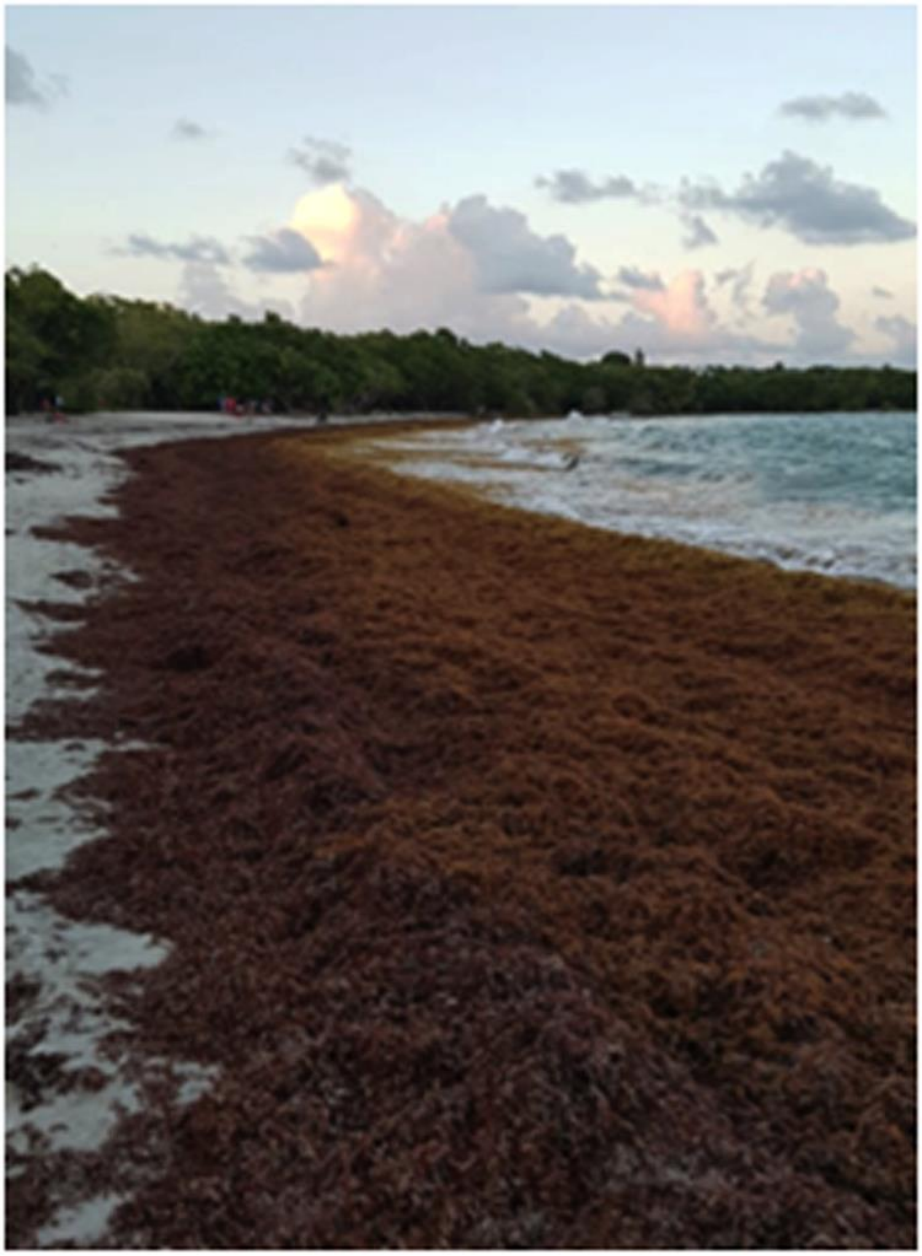

Figure 1. Sargassum spp. accumulation on Saint-Felix beach, Guadeloupe Island(French Antilles)

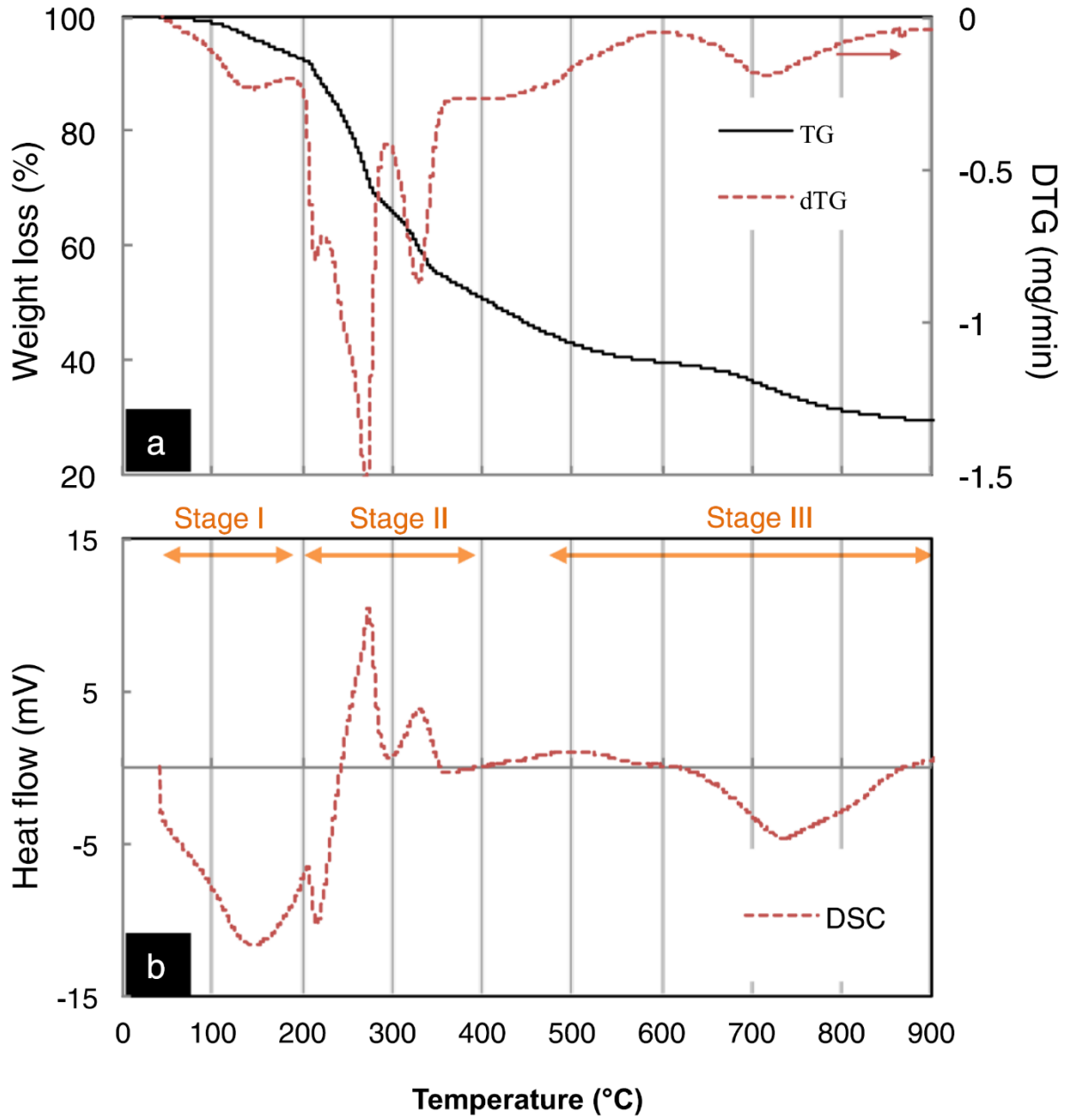

Figure 2. Thermogravimetric plots of Sargassum spp. precursor (a) TGA and DTG, (b) DSC.

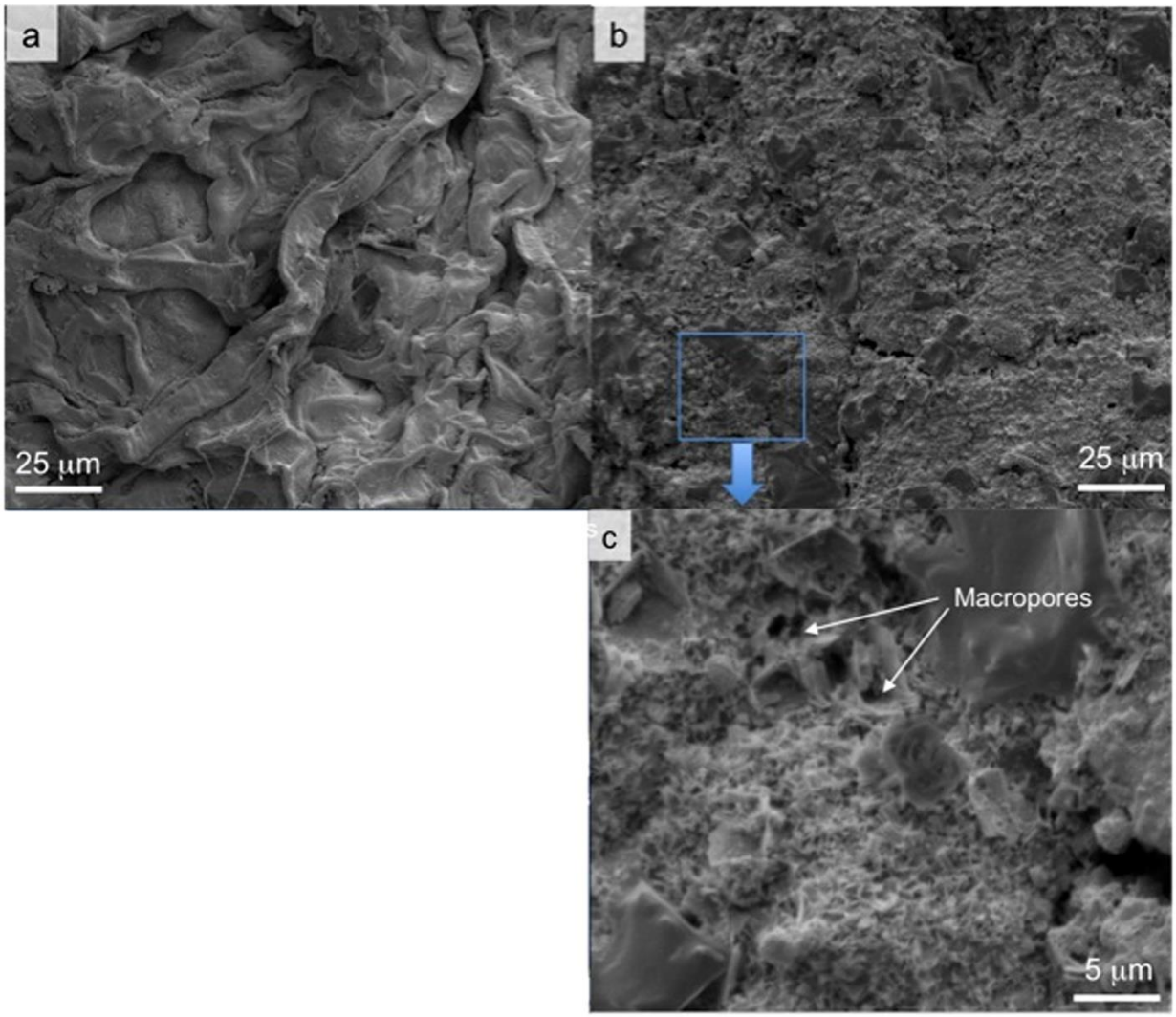

Figure 3. SEM images of Sargassum spp. before (a), after (b, c) pyrolysis at 700°C.

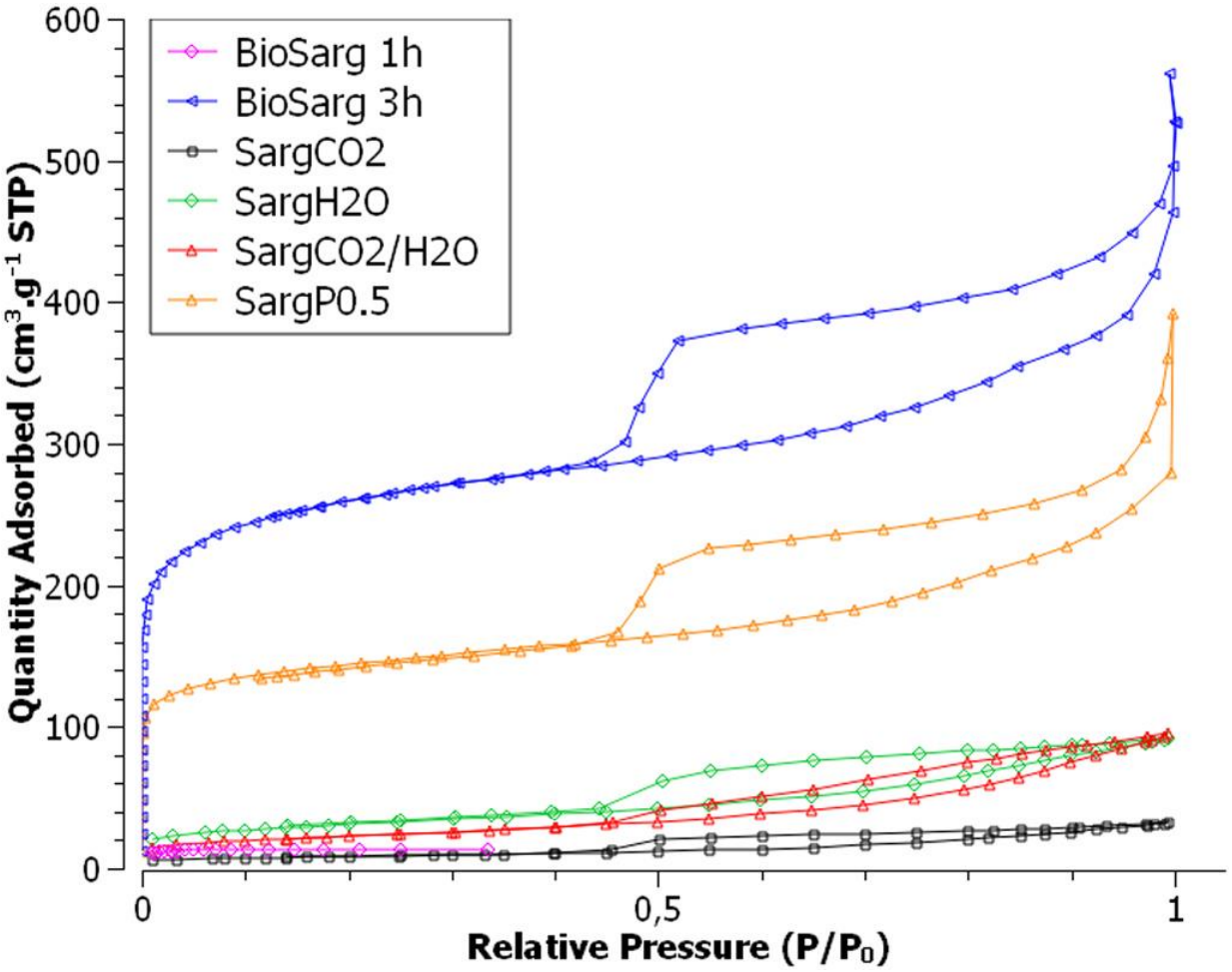

Figure 4. N_2 adsorption-desorption isotherms of Sargassum spp. BCs (BioSarg 1h, BioSarg 3h) and ACs ($SargCO_2$, $SargH_2O$, $SargCO_2/H_2O$ and SargP0.5).

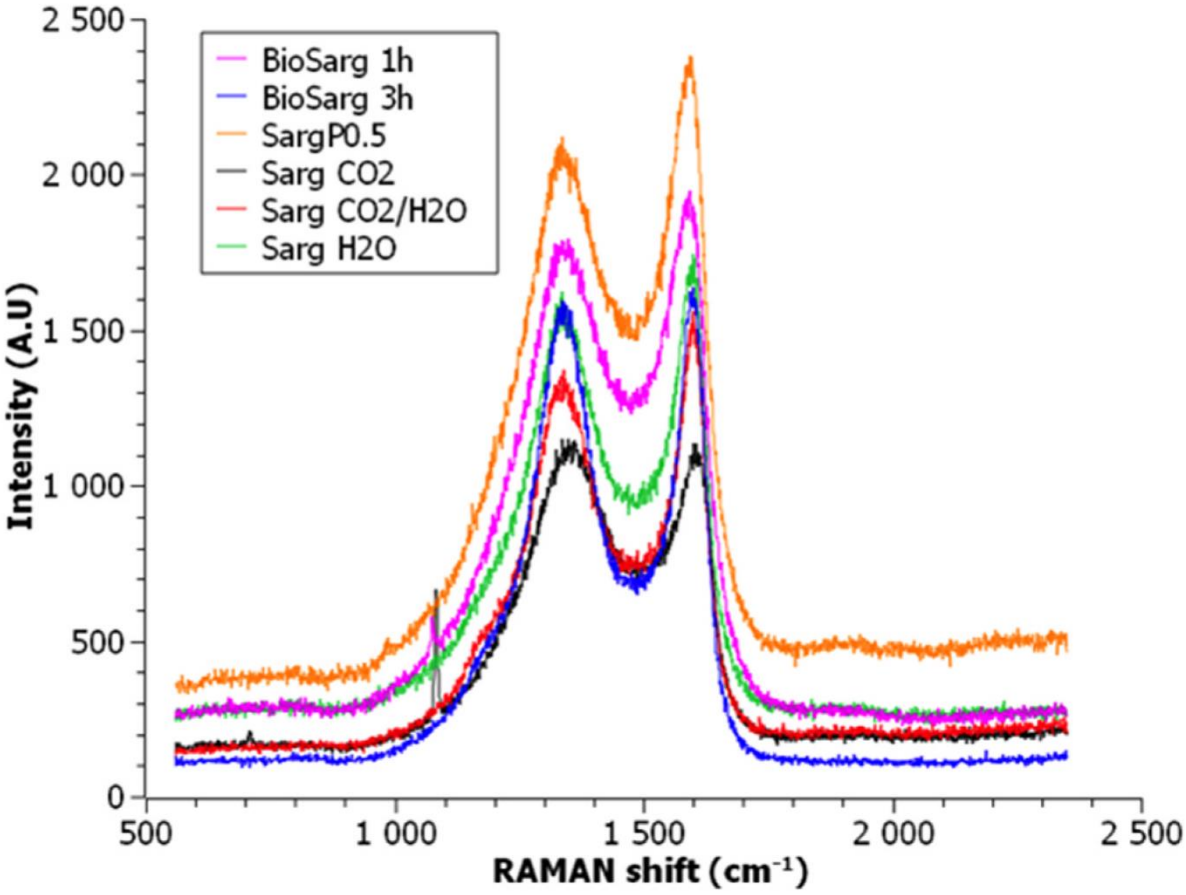

Figure 5. RAMAN spectra of Sargassum *spp*. BCs and ACs.

Indication: Numbers correspond to the PCB congeners. Framed congeners are dioxin-like PCBs. Bold numbers were congeners transferred at a high level ranking from 38 to 78% and from 30 to 80% respectively for milk and eggs.

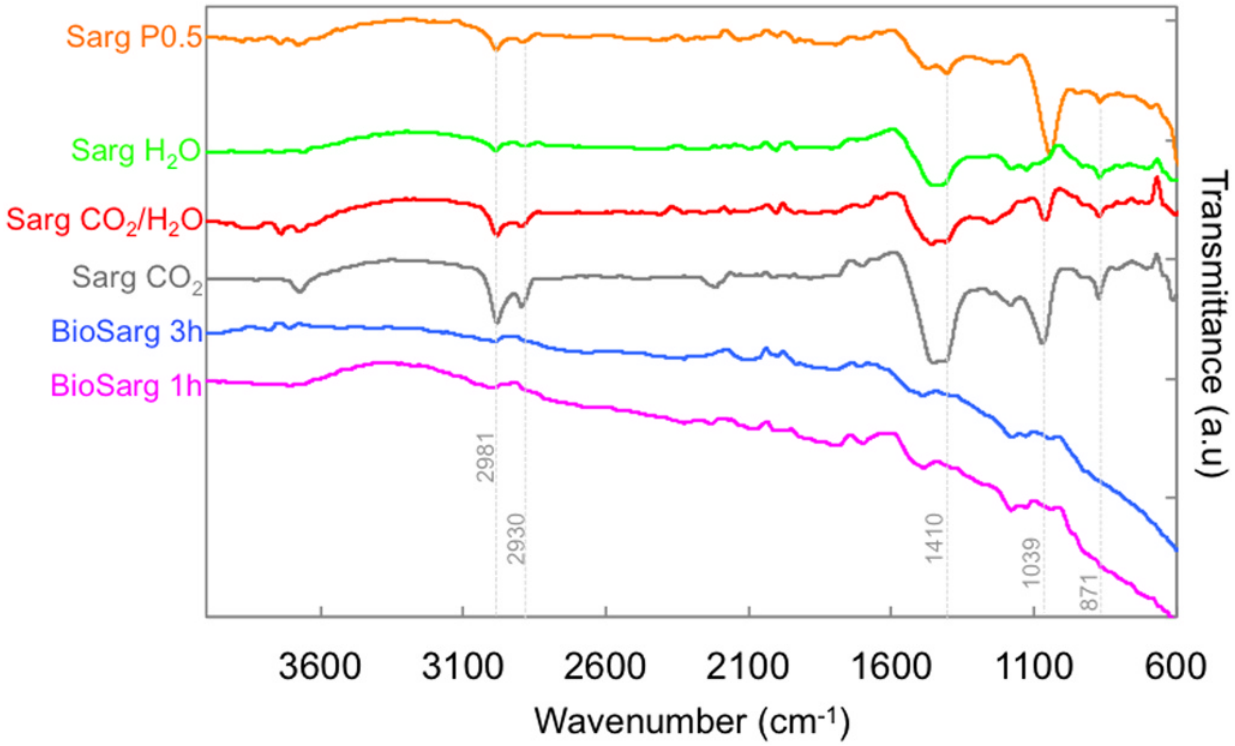

Figure 6. FT-IR spectra of Sargassum *spp*. based samples: biochars BCs (BioSarg1h, BioSarg 3h) and activated carbons ACs (SargCO2, SargH2O, SargCO2/ H2O and SargP0.5).

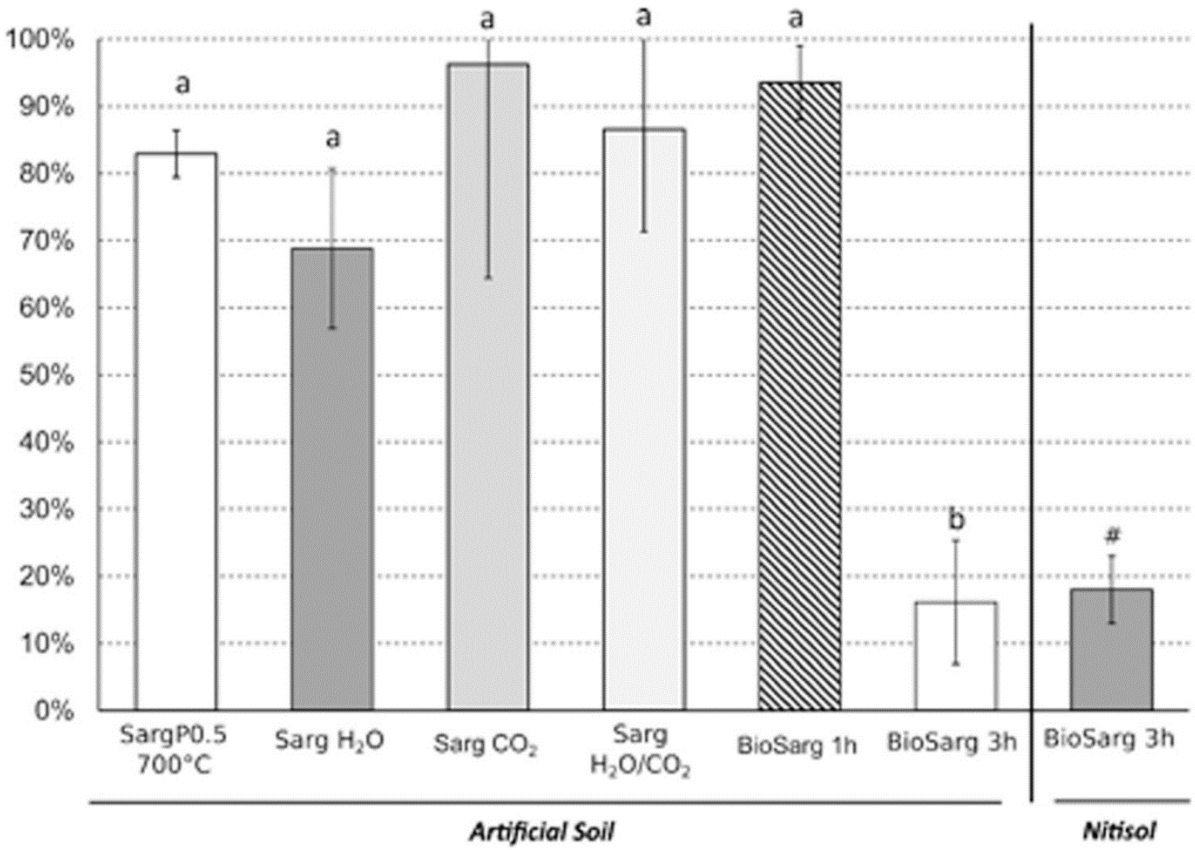

Figure 5. CLD availability in OECD artificial soil and Nitisol. CLD availability is expressed in % of CLD availability of corresponding soil without amendment (n = 6).

Values correspond to the mean ± SD (n = 3). Mean values with different superscript letters (a, b) are statistically different (P < 0.05). #: Amended Nitisol presented significantly reduced levels (p < 0.001) compare to Nitisol without amendment. Statistical analysis was performed using the one-way ANOVA procedure of R software and Tukey post-hoc test.

5. References

[1] J.P. Mar´echal, C. Hellio, C. Hu, A simple, fast, and reliable method to predict Sargassum washing ashore in the Lesser Antilles, Remote Sens. Appl. Soc. Environ. 5 (2017) 54–63, https://doi.org/10.1016/j.rsase.2017.01.001.

[2] K. Britton-Simmons, Direct and indirect effects of the introduced alga Sargassum muticum on benthic, subtidal communities of Washington State, USA, Mar. Ecol. Prog. Ser. 277 (2004) 61–78, https://doi.org/10.3354/meps277061.

[3] C. Louime, J. Fortune, G. Gervais, Sargassum invasion of coastal environments: a growing concern, Am. J. Environ. Sci. 13 (2017) 58–64, https://doi.org/10.3844/ ajessp.2017.58.64.

[4] B. Gavio, M.N. Rinc´on-Díaz, A. Santos-Martínez, Cantidades masivas de Sargassum pel´agicos en las costas de San Andr´es Isla, Caribe suroccidental, Acta Biol. Colomb. 20 (2015) 239–241, https://doi.org/10.15446/abc.v20n1.46109.

[5] V. Smetacek, A. Zingone, Green and golden seaweed tides on the rise, Nature 504 (2013) 84–88, https://doi.org/10.1038/nature12860.

[6] M. Wang, C. Hu, Predicting Sargassum blooms in the Caribbean sea from MODIS observations, Geophys. Res. Lett. 44 (2017) 3265–3273, https://doi.org/10.1002/ 2017GL072932.

[7] Y.-M. Cabidoche, R. Achard, P. Cattan, C. Clermont-Dauphin, F. Massat, J. Sansoulet, Long-term pollution by chlordecone of tropical volcanic soils in the French West Indies: a simple leaching model accounts for current residue, Environ. Pollut. 157 (2009) 1697–1705, https://doi.org/10.1016/j.envpol.2008.12.015.

[8] E.E. Kenaga, Predicted bioconcentration factors and soil sorption coefficients of pesticides and other chemicals, Ecotoxicol. Environ. Saf. 4 (1980) 26–38, https:// doi.org/10.1016/0147-6513(80)90005-6.

[9] P.H. Howard, Handbook of environmental degradation rates, CRC Press, 1991

[10] S. Coat, D. Monti, P. Legendre, C. Bouchon, F. Massat, G. Lepoint, Organochlorine pollution in tropical rivers (Guadeloupe): Role of ecological factors in food web bioaccumulation, Environ. Pollut. 159 (2011) 1692–1701, https://doi.org/ 10.1016/j.envpol.2011.02.036.

[11] Y.-M. Cabidoche, M. Lesueur-Jannoyer, Contamination of harvested organs in root crops grown on chlordecone-polluted soils, Pedosphere 22 (2012) 562–571, https://doi.org/10.1016/S1002-0160(12)60041-1.

[12] Y. Yue, C. Shen, Y. Ge, Biochar accelerates the removal of tetracyclines and their intermediates by altering soil properties, J. Hazard. Mater. 380 (2019), 120821.

[13] L. Xiang, H. Sheng, C. Gu, R.-G. Marc, Y. Wang, Y. Bian, X. Jiang, F. Wang, Biochar combined with compost to reduce the mobility, bioavailability and plant uptake of 2,2′,4,4′-tetrabrominated diphenyl ether in soil, J. Hazard. Mater. 374 (2019) 341–348, https://doi.org/10.1016/j.jhazmat.2019.04.048.

[14] X. You, H. Jiang, M. Zhao, F. Suo, C. Zhang, H. Zheng, K. Sun, G. Zhang, F. Li, Y. Li, Biochar reduced Chinese chive (Allium tuberosum) uptake and dissipation of thiamethoxam in an agricultural soil, J. Hazard. Mater. 390 (2020), 121749, https://doi.org/10.1016/j.jhazmat.2019.121749.

[15] K. Karhu, T. Mattila, I. Bergstr¨om, K. Regina, Agriculture, ecosystems and environment biochar addition to agricultural soil increased CH4 uptake and water holding capacity – Results from a short-term pilot field study, Agric. Ecosyst. Environ. 140 (2011) 309–313, https://doi.org/10.1016/j.agee.2010.12.005.

[16] Y.-P. Yang, X.-J. Tang, H.-M. Zhang, W.-D. Cheng, G.-L. Duan, Y.-G. Zhu, The characterization of arsenic biotransformation microbes in paddy soil after straw biochar and straw amendments, J. Hazard. Mater. 391 (2020), 122200, https://doi.org/10.1016/j.jhazmat.2020.122200.

[17] B. Mandal, H. Bhattacharjee, N. Mittal, H. Sah, P. Balabathula, L.A. Thoma, G.
C. Wood, Core–shell-type lipid–polymer hybrid nanoparticles as a drug delivery platform, Nanomed. Nanotechnol. Biol. Med. 9 (2013) 474–491, https://doi.org/ 10.1016/j.nano.2012.11.010.
[18] S. Mandal, R. Thangarajan, N.S. Bolan, B. Sarkar, N. Khan, Y.S. Ok, R. Naidu, Biochar-induced concomitant decrease in ammonia volatilization and increase in nitrogen use efficiency by wheat, in: Biochars Multifunctional Role as a Novel Technology in the Agricultural, Environmental, and Industrial Sectors., 2016, pp. 73–89. http://www.sciencedirect.com/science/article/pii/S0045653515004 3 24.
[19] S. Yehya, M. Delannoy, A. Fournier, M. Baroudi, G. Rychen, C. Feidt, Activated carbon, a useful medium to bind chlordecone in soil and limit its transfer to growing goat kids, PLOS One 12 (2017), e0179548, https://doi.org/10.1371/ journal.pone.0179548.
[20] M. Delannoy, D. Techer, S. Yehya, A. Razafitianamaharavo, F. Amutova, A. Fournier, M. Baroudi, E. Montarges-Pelletier, G. Rychen, C. Feidt, Evaluation of two contrasted activated carbon-based sequestration strategies to reduce soil-bound chlordecone bioavailability in piglets, Environ. Sci. Pollut. Res. (2019), https://doi.org/10.1007/s11356-019-06494-z.
[21] R. Ranguin, C. Jean-Marius, C. Yacou, S. Gaspard, C. Feidt, G. Rychen,
M. Delannoy, Reduction of chlordecone environmental availability by soil amendment of biochars and activated carbons from lignocellulosic biomass, Environ. Sci. Pollut. Res. 27 (2020) 41093–41104, https://doi.org/10.1007/ s11356-019-07366-2.
[22] S. Altenor, B. Carene, E. Emmanuel, J. Lambert, J.J. Ehrhardt, S. Gaspard, Adsorption studies of methylene blue and phenol onto vetiver roots activated carbon prepared by chemical activation, J. Hazard. Mater. 165 (2009) 1029–1039, https://doi.org/10.1016/j.jhazmat.2008.10.133.
[23] E.J. Soltes, T.J. Elder, Pyrolysis in organic chemicals from biomass, CRC Press, Goldstein Fla, 1981.
[24] E. Raymundo-Pi˜nero, M. Cadek, F. B´eguin, Tuning carbon materials for supercapacitors by direct pyrolysis of seaweeds, Adv. Funct. Mater. 19 (2009) 1032–1039, https://doi.org/10.1002/adfm.200801057.
[25] Z. Tian, Y. Qiu, J. Zhou, X. Zhao, J. Cai, The direct carbonization of algae biomass to hierarchical porous carbons and CO2 adsorption properties, Mater. Lett. 180 (2016) 162–165, https://doi.org/10.1016/j.matlet.2016.05.169.
[26] M.C. Ncibi, V. Jeanne-Rose, B. Mahjoub, C. Jean-Marius, J. Lambert, J.J. Ehrhardt, Y. Bercion, M. Seffen, S. Gaspard, Preparation and characterisation of raw chars and physically activated carbons derived from marine Posidonia oceanica (L.) fibres, J. Hazard. Mater. 165 (2009) 240–249.
[27] C.-F. Chang, C.-Y. Chang, W.-T. Tsai, Effects of Burn-off and Activation Temperature on Preparation of Activated Carbon from Corn Cob Agrowaste by CO2 and Steam, J. Colloid Interface Sci. 232 (2000) 45–49, https://doi.org/10.1006/ jcis.2000.7171.
[28] S. Gaspard, S. Altenor, E.A. Dawson, P.A. Barnes, A. Ouensanga, Activated carbon from vetiver roots: gas and liquid adsorption studies, J. Hazard. Mater. 144 (2007) 73–81, https://doi.org/10.1016/j.jhazmat.2006.09.089.
[29] S. Brunauer, P.H. Emmett, E. Teller, Adsorption of gases in multimolecular layers, J. Am. Chem. Soc. 60 (1938) 309–319, https://doi.org/10.1021/ja01269a023.
[30] F. Stoeckli, M.V. L´opez-Ram´on, D. Hugi-Cleary, A. Guillot, Micropore sizes in activated carbons determined from the Dubinin–Radushkevich equation, Carbon 39 (2001) 1115–1116, https://doi.org/10.1016/S0008-6223(01)00054-9.
[31] E.P. Barrett, L.G. Joyner, P.P. Halenda, The determination of pore volume and area distributions in porous substances. I. computations from nitrogen isotherms, J. Am. Chem. Soc. 73 (1951) 373–380, https://doi.org/10.1021/ja01145a126.
[32] M. Luisa Ojeda, J. Marcos Esparza, A. Campero, S. Cordero, I. Kornhauser, F. Rojas, On comparing BJH and NLDFT pore-size distributions determined from N2 sorption on SBA-15 substrata, Phys. Chem. Chem. Phys. 5 (2003) 1859–1866, https://doi.org/10.1039/b300821e.
[33] OECD, Test no 207 earthworm acute toxicity test, in: Effects on Biotic Systems, OECD Publishing, Paris, 1984, https://doi.org/10.1787/20745761.
[34] S. Jurjanz, C. Jondreville, M. Mahieu, A. Fournier, H. Archim`ede, G. Rychen, C. Feidt, Relative bioavailability of soil-bound chlordecone in growing lambs, Environ. Geochem. Health 36 (2014) 911–917, https://doi.org/10.1007/s10653-014-9608-5.
[35] C. Yacou, S. Altenor, B. Carene, S. Gaspard, Chemical structure investigation of tropical Turbinaria turbinata seaweeds and its derived carbon sorbents applied for the removal of hexavalent chromium in water, Algal Res. 34 (2018) 25–36, https:// doi.org/10.1016/j.algal.2018.06.014.
[36] K.K.A. Sanjeewa, N. Kang, G. Ahn, Y. Jee, Y.-T. Kim, Y.-J. Jeon, Bioactive potentials of sulfated polysaccharides isolated from brown seaweed Sargassum spp in related to human health applications: a review, Food Hydrocoll. 81 (2018) 200–208, https://doi.org/10.1016/j.foodhyd.2018.02.040.
[37] S. Yende, B. Chaugule, U. Harle, Therapeutic potential and health benefits of Sargassum species, Pharmacogn. Rev. 8 (2014) 1, https://doi.org/10.4103/0973-7847.125514.
[38] N. Ye, D. Li, L. Chen, X. Zhang, D. Xu, Comparative studies of the pyrolytic and kinetic characteristics of maize straw and the seaweed ulva pertusa, PLoS One 5 (2010), e12641, https://doi.org/10.1371/journal.pone.0012641.
[39] I. Ali, A. Bahadar, Red Sea seaweed (Sargassum spp.) pyrolysis and its devolatilization kinetics, Algal Res 21 (2017) 89–97, https://doi.org/10.1016/j. algal.2016.11.011.
[40] R.C. Oliveira, P. Hammer, E. Guibal, J.-M. Taulemesse, O. Garcia, Characterization of metal–biomass interactions in the lanthanum(III) biosorption on Sargassum sp. using SEMØX, FTIR, and XPS: Preliminary studies, Chem. Eng. J. 239 (2014) 381–391, https://doi.org/10.1016/j.cej.2013.11.042.
[41] J.C.P. Broekhoff, J.H. De Boer, Studies on pore systems in catalysts. XI. Pore distribution calculations from the adsorption branch of a nitrogen adsorption isotherm in the case of “ink-bottle” type pores, J. Catal. 10 (1968) 153–165, https://doi.org/10.1016/0021-9517(68)90168-1.
[42] M. Nakamizo, R. Kammereck, P.L. Walker, Laser raman studies on carbons, Carbon 12 (1974) 259–267, https://doi.org/10.1016/0008-6223(74)90068-2.
[43] M.S. Dresselhaus, P.C. Eklund, Phonons in carbon nanotubes, Adv. Phys. 49 (2000) 705–814, https://doi.org/10.1080/000187300413184.
[44] M.S. Dresselhaus, G. Dresselhaus, R. Saito, A. Jorio, Raman spectroscopy of carbon nanotubes, Phys. Rep. 409 (2005) 47–99, https://doi.org/10.1016/j. physrep.2004.10.006.
[45] I.B. Yanchuk, M.Y. Valakh, A.Y. Vul', V.G. Golubev, S.A. Grudinkin, N.A. Feoktistov, A. Richter, B. Wolf, Raman scattering, AFM and nanoindentation characterisation of diamond films obtained by hot filament CVD, Diam. Relat. Mater. 13 (2004) 266–269, https://doi.org/10.1016/j.diamond.2003.11.001.
[46] J.M. Holden, P. Zhou, X.-X. Bi, P.C. Eklund, S. Bandow, R.A. Jishi, K. Das Chowdhury, G. Dresselhaus, M.S. Dresselhaus, Raman scattering from nanoscale carbons generated in a cobalt-catalyzed carbon plasma, Chem. Phys. Lett. 220 (1994) 186–191, https://doi.org/10.1016/0009-2614(94)00154-5.
[47] G. Lalwani, A.M. Henslee, B. Farshid, L. Lin, F.K. Kasper, Y.-X. Qin, A.G. Mikos, B. Sitharaman, Two-dimensional nanostructure-reinforced biodegradable polymeric nanocomposites for bone tissue engineering, Biomacromolecules 14 (2013) 900–909, https://doi.org/10.1021/bm301995s.
[48] S. Biniak, A. ´Swiątkowski, M. Pakuła, M. Sankowska, K. Ku´smierek, G. Trykowski, Cyclic voltammetric and FTIR studies of powdered carbon electrodes in the electrosorption of 4-chlorophenols from aqueous electrolytes, Carbon 51 (2013) 301–312, https://doi.org/10.1016/j.carbon.2012.08.057.
[49] X. Han, Y. He, H. Zhao, D. Wang, Optimization of preparation conditions of activated carbon from the residue of desilicated rice husk using response surface methodology, Korean J. Chem. Eng. 31 (2014) 1810–1817, https://doi.org/ 10.1007/s11814-014-0103-6.
[50] K. Bilba, A. Ouensanga, Fourier transform infrared spectroscopic study of thermal degradation of sugar cane bagasse, J. Anal. Appl. Pyrolysis 38 (1996) 61–73, https://doi.org/10.1016/S0165-2370(96)00952-7.
[51] D. Iruretagoyena, K. Bikane, N. Sunny, H. Lu, S.G. Kazarian, D. Chadwick, R. Pini, N. Shah, Enhanced selective adsorption desulfurization on CO2 and steam treated activated carbons: equilibria and kinetics, Chem. Eng. J. 379 (2020), 122356, https://doi.org/10.1016/j.cej.2019.122356.
[52] L. Yang, T. Huang, X. Jiang, W. Jiang, Effect of steam and CO2 activation on characteristics and desulfurization performance of pyrolusite modified activated carbon, Adsorption 22 (2016) 1099–1107, https://doi.org/10.1007/s10450-016-9832-7.
[53] T. Wigmans, Industrial aspects of production and use of activated carbons, Carbon 27 (1989) 13–22, https://doi.org/10.1016/0008-6223(89)90152-8.
[54] K. L´aszl´o, E. Tomb´acz, K. Josepovits, Effect of activation on the surface chemistry of carbons from polymer precursors, Carbon 39 (2001) 1217–1228, https://doi. org/10.1016/S0008-6223(00)00245-1.
[55] C.L. Mangun, K.R. Benak, M.A. Daley, J. Economy, Oxidation of activated carbon fibers: effect on pore size, surface chemistry, and adsorption properties, Chem. Mater. 11 (1999) 3476–3483.
[56] M. Ehara, K. Kuramoto, H. Nakatsuji, M. Hoshino, T. Tanaka, M. Kitajima, H. Tanaka, A. De Fanis, Y. Tamenori, K. Ueda, C1s and O1s photoelectron satellite spectra of CO with symmetry-

dependent vibrational excitations, J. Chem. Phys. 125 (2006), 114304, https://doi.org/10.1063/1.2346683.
[57] B.P. Payne, M.C. Biesinger, N.S. McIntyre, X-ray photoelectron spectroscopy studies of reactions on chromium metal and chromium oxide surfaces, J. Electron Spectrosc. Relat. Phenom. 184 (2011) 29–37, https://doi.org/10.1016/j. elspec.2010.12.001.
[58] J.A. Maci´a-Agull´o, D. Cazorla-Amor´os, A. Linares-Solano, U. Wild, D.S. Su,R. Schl ¨ogl, Oxygen functional groups involved in the styrene production reaction
[59] M. Delannoy, S. Yehya, D. Techer, A. Razafitianamaharavo, A. Richard, G. Caria, M. Baroudi, E. Montarg`es-Pelletier, G. Rychen, C. Feidt, Amendment of soil by biochars and activated carbons to reduce chlordecone bioavailability in piglets, Chemosphere 210 (2018) 486–494, https://doi.org/10.1016/j. chemosphere.2018.05.181.
[60] A. Durimel, S. Altenor, R. Miranda-Quintana, P. Couespel Du Mesnil, U. Jauregui-Haza, R. Gadiou, S. Gaspard, pH dependence of chlordecone adsorption on activated carbons and role of adsorbent physico-chemical properties, Chem. Eng. J. 229 (2013) 239–249, https://doi.org/10.1016/j.cej.2013.03.036.
[61] A. Durimel, N. Pass´e-Coutrin, C. Jean-Marius, R. Gadiou, C. Enriquez-Victorero, D. Hern´andez-Vald´es, U. Jauregui-Haza, S. Gaspard, Role of acidic sites in beta-hexachlorocyclohexane (β-HCH) adsorption by activated carbons: molecular modelling and adsorption–desorption studies, RSC Adv. 5 (2015) 85153–85164.